

## Raman line shapes from sputtered thin films of $\text{Y}(\text{Pr})\text{Ba}_2\text{Cu}_3\text{O}_{6+\delta}$ : Fine structures and oxygen ordering

Eric Faulques and Victor G. Ivanov\*

*Laboratoire de Physique Cristalline, Institut des Matériaux de Nantes, 2 rue de la Houssinière, F-44072 Nantes Cedex 03, France*

(Received 10 May 1996; revised manuscript received 1 August 1996)

A temperature dependence study of Raman line shapes taken from superconducting and insulating  $\text{Y}(\text{Pr})\text{Ba}_2\text{Cu}_3\text{O}_{6+\delta}$  thin films with well-characterized electrophysical properties and morphologies ( $a$ -axis or  $c$ -axis orientation) has been carried out using the excitation energies at 1.83 eV and 2.41 eV. Ba and Cu bands show doublets, with 113–119  $\text{cm}^{-1}$  and 146–152  $\text{cm}^{-1}$  components and have been calculated using a Green's function model. The shapes of the 113 and 152  $\text{cm}^{-1}$  lines are well described by Lorentzians whereas those of the other two components can be satisfactorily reproduced in the assumption that two phonons of bare frequencies 119 and 146  $\text{cm}^{-1}$  interact with a *common* continuum of excitations. The temperature dependence of the phonon-continuum coupling parameters allows us to ascribe the scattering continuum to low-energy electronic interband transitions. The model is able to explain qualitatively the overestimated mixing between pure Ba and plane  $\text{Cu } A_g$  vibrational modes found in previous first-principles calculations. We also find that for the 1.83 eV exciting line, the  $B_{1g}$  oxygen phonon at 335  $\text{cm}^{-1}$  presents a strong Fano effect and anomalous temperature dependence. We link Raman features occurring at  $\approx 220$ –240, 270–290, and 560–596  $\text{cm}^{-1}$  to the existence of *local* variations in oxygen composition resulting from the conditions of deposition. These lines could originate from chain defects and be activated by a coupling between  $A_g$  and  $B_{2g}$ - $B_{3g}$  modes. The presence of microphases of oxygen-depleted domains (ortho-II phase) reproducing macroscopic oxygen disorder is proposed. [S0163-1829(97)03405-X]

### I. INTRODUCTION

The Raman effect in  $\text{Y}(\text{Pr})\text{Ba}_2\text{Cu}_3\text{O}_{6+\delta}$  (YBCO) has proved to be very efficient for probing vibrations of the cationic and oxygen sublattices in these materials.<sup>1</sup> Although the Raman spectra of these systems have been well documented in the literature for sintered samples and single crystals, little work has been devoted to the systematic Raman study of thin sputtered films in relation to the growth conditions. Thin films are the best candidates for industrial applications, especially for superlattices, tunnel-Josephson-junction devices, and have provided the best critical currents  $J_c$  thus far. Therefore, considerable effort is warranted in order to better characterize them using contact-free techniques such as light scattering. Substrate temperature, plasma composition, sputtering geometry, and epitaxy are essential data for optimizing film properties. Raman probes can provide valuable *in situ* data in the reactor during the epitaxial growth and may be useful at various processing stages. The strong anisotropic nature of thin films, which may be considered as quasi-two-dimensional systems, is particularly interesting for Raman measurements which are symmetry dependent.

Some of the more advantageous properties of the films for Raman experiments over other samples are a thickness of the order of the penetration depth of the light (thus probing not only the surface as in single crystals but also the bulk), the quasiperfect scattering geometry due to the large planar surface available for the beam spot, and the highly preferential epitaxial orientation with respect to the substrate.<sup>2,3</sup> A characteristic of the present work is the large number of recorded data points which has increased the resolution of the experiment over previous investigations.

A special issue developed in this work concerns the Fano interference phenomenon<sup>4–6</sup> which has been observed in the superconducting  $\text{YBa}_2\text{Cu}_3\text{O}_{6+\delta}$  by Thomsen *et al.*<sup>7</sup> and Cooper *et al.*<sup>8</sup> for the  $B_{1g}$ -like phonon at 340  $\text{cm}^{-1}$ . The significance of this finding is that it proves the existence of intrinsic scattering background in this material, and interaction between the phonon which exhibits the Fano asymmetry and the elementary excitations from the continuum. The Raman scattering of our films has provided an opportunity to study this effect with great detail.

A well-pronounced, symmetric Lorentzian profile of the 340  $\text{cm}^{-1}$  line in  $\text{YBa}_2\text{Cu}_3\text{O}_6$  (Ref. 9) and  $\text{PrBa}_2\text{Cu}_3\text{O}_7$  (Ref. 10) samples, is a signature for background fading in the semiconducting state, and serves a strong evidence in favor of its electronic origin.

Another phonon in  $\text{YBa}_2\text{Cu}_3\text{O}_{6+\delta}$  which exhibits a strong asymmetry is the  $\approx 115 \text{ cm}^{-1}$   $A_g$  mode, which is usually ascribed to Ba vibrations along the  $c$  crystallographic axis. The origin of the scattering background which interacts with this vibration is less clear. It was demonstrated,<sup>11</sup> that the asymmetric profile of the 115  $\text{cm}^{-1}$  mode persists even at temperatures much lower than that of the superconducting transition, where an energy gap  $2\Delta > 300 \text{ cm}^{-1}$  in the electronic excitation spectrum is expected to be opened.<sup>12</sup> Later, Bogatchev *et al.*<sup>13</sup> observed that the asymmetry of this mode is preserved through the whole range of rare earth substitution in the  $R_{0.5}\text{Pr}_{0.5}\text{Ba}_2\text{Cu}_3\text{O}_{6+\delta}$  system. These experiments show that the scattering continuum which interacts with Ba vibrations is of origin different from that of the continuum which interferes with the O(2)-O(3) out-of-phase vibrations, and probably is not connected entirely with the conducting electrons in the  $\text{CuO}_2$  planes.

TABLE I. Electrophysical parameters of some films used for this study.  $H$  and  $Y$  refer, respectively, to out-of-axis and in-axis sputtering,  $P$  to insulating Pr cuprates. Films  $H1$  and  $Y4$  are grown on  $\text{SrTiO}_3$  substrates, the others are deposited on  $\text{MgO}$  substrates.  $T_0$  indicates the onset of superconductivity,  $T_s$  the temperature of the substrate, and the  $\perp$  axis the orientation with respect to the substrate.  $p_0$  is the oxygen partial pressure expressed in percentage of the total plasma pressure  $p_T$  and  $h$  is the film thickness.

Film	$T_s$ (°C)	$p_T$ (Pa)	$p_0$ (%)	$\perp$ axis	$c$ (Å)	$h$ (Å)	Ba:Cu	$T_0$ (K)	$T_c$ (K)	$J_c$ (MA/cm <sup>2</sup> )
$H1$	740	80	33	$c$	11.73	3000	2:3	92	90.8	$\leq 5$
$H2$	650/750	80	33	$a(95\%)$	11.71	2000	—	90	79	$\leq 2$
$H3$	640	80	33	$a(80\%)$	11.71	3000	—	86	12	—
$Y1$	660	80	10	$c$	11.75	1200	2:3.1	89	62	—
$Y2$	660	26.6	4	$c$	11.78	2700	2.2:3.8	67	63	—
$Y3$	680	26.6	52	$c+a$	11.93	2700	2:2.6	75	45	—
$Y4$	745	66.5	10	$c$	11.70	1000	2.3:4.2	91	87.5	$\leq 1$
$Y5$	740	66.5	20	$c$	11.70	1500	2.2:3.3	86	81.4	$\leq 2$
$Y6$	740	66.5	25	$c$	11.69	1400	1.9:2.9	89	84.8	$\leq 1$
$Y7$	715	66.5	25	$c$	11.70	—	1.9:3.2	88	81.5	$\leq 1$
$Y8$	740	66.5	25	$c$	11.68	—	2.3:3.1	89	84.8	0.05 <sup>a</sup>
$P4$	645	26.6	10	$a(97\%)$	12.16	4200	2.6:3.7	—	—	—
$P7$	725	26.6	25	$c$	11.72	2400	2.2:3.6	—	—	—
$P10$	660	26.6	40	$a(85\%)$	11.70	1600	2.5:4.8	—	—	—
$P11$	655	26.6	4	$a(90\%)$	—	1600	2.5:4.8	—	—	—

<sup>a</sup>At 4 K, other  $J_c$ 's taken at 77 K.

In this context, an opened issue in the Raman spectroscopy of YBCO-type compounds is the degree of mixing of the Ba and plane Cu vibrations in the modes at  $\approx 115$  and  $\approx 150$   $\text{cm}^{-1}$ .  $^{65}\text{Cu}$ - $^{63}\text{Cu}$  isotopic substitution experiments,<sup>14,15</sup> as well as resonant Raman spectroscopy<sup>16</sup> give a value of less than 20%, while *ab initio* calculations of the lattice dynamics of  $\text{YBa}_2\text{Cu}_3\text{O}_7$  (Ref. 17 and 18) lead to nearly 50 % mixing.

The present paper was motivated by the observation that a simple superposition of a Fano line profile for the  $\approx 115$   $\text{cm}^{-1}$  band, and a Lorentzian for the  $\approx 150$   $\text{cm}^{-1}$  one, can not adequately describe the valley in the scattering intensity between the two lines. We demonstrate that a satisfactory fit to the experimental spectra may be obtained, if one assumes that Ba and Cu  $A_g$  vibrations interact with a common continuum of excitations.

Experimental conditions and nature of the films are given in Sec. II. The model of interaction between the Ba and Cu lines and a continuum is described in Sec. III. In Sec. IV we present our experimental data obtained at low temperature by using a low-energy excitation laser line in off-resonance conditions at 1.83 eV and the corresponding theoretical fits. We draw possible implications of the model for the electronic structure and electron-phonon coupling in YBCO-type materials. The change of the phonon at 335  $\text{cm}^{-1}$  which shows anomalous scattering of the Cu-O bond bending mode is also described in this section. In Sec. V, we point out that sputtered films exhibit an oxygen sublattice disorder at a macroscopic scale pictured by activation of strong Raman-forbidden lines (infrared allowed) at 220–240, 562, and 596  $\text{cm}^{-1}$  which are distinct from in-plane vibrational modes of  $B_{2g}$  and  $B_{3g}$  symmetries.

## II. EXPERIMENTAL DETAILS

### A. Physical properties of thin films

All films used in this study were obtained by cathodic magnetron sputtering, a technique which gives a smooth layer on substrates with large surface. Their fabrication and their physical properties have been described in previously published papers by Garz and Gonzalez.<sup>19</sup> Table I lists the available electrophysical parameters of these films as given by these authors. Most films have thickness ranging from 1000 to 3000 Å and have relatively high transition-temperature onsets. Some films of the  $Y$  and  $P$  series exhibit a stoichiometry with an excess of copper. The  $J_c$ 's are satisfactory. The films are grown with either the  $c$  axis or  $a$  axis perpendicular to the substrate plane (denoted in the following by  $c$  axis or  $a$  axis or  $a\perp$  and  $c\perp$ ). The  $a\perp$  films are obtained with a substrate temperature  $T_s$  lying between 640 and 660 °C (low-temperature process). When 670 °C  $< T_s < 715$  °C the film grows with mixed  $a\perp$  and  $c\perp$  orientations. If 720 °C  $< T_s < 790$  °C one observes only the  $c\perp$  orientation. The YBCO film  $H2$  has been synthesized using the two-stage process: a YBCO buffer layer is first deposited at low temperature during 5–15 min followed by a slope to a higher temperature with a plateau. Then,  $T_s$  is lowered towards 450 °C where the sample is oxygenated at higher oxygen pressure during 20 min.

The  $a$  and  $c$  lattice parameters have been obtained with the (200) and (007) lines of the x-ray diffraction (XRD) pattern. The  $a$  and  $c$  values are in all cases larger than those determined for bulk materials (3.82 and 11.68 Å, respectively). The elongated  $c$  parameter is related to weak orthorhombicity. For  $c$ -axis films it was found that 3.843 Å  $< a < 3.917$  Å.

The epitaxy in the plane of growth has been determined by Buerger precession and by  $\phi$ -scan XRD for films on MgO (100) substrate and for the other substrates, respectively. The grains of  $c$ -axis films grown on the SrTiO<sub>3</sub> (100) substrate have  $a$  and  $b$  axes aligned with those of the substrate plane, i.e., at 0° orientation.  $c$ -axis films grown on a MgO substrate have  $a$  and  $b$  axes rotated 0° or 45° to MgO axes. In particular, films *H1* and *Y4* present a perfect epitaxy, and the  $b$  and  $c$  axes of *H2* and *H3* ( $a$ -axis films) are oriented at 45° with respect to the  $a$  axis of MgO. The insulating praseodymium  $a$ -axis films *P4*, *P10*, and *P11* have grains with  $b$  and  $c$  axes aligned with those of MgO (0° orientation). The  $c$ -axis film *P7* has crystallites with 0°, 45°, and 90° epitaxy.

### B. Measurements

The low-temperature measurements were conducted from 10 K to 293 K at  $\pm 0.5$  K and recorded from an optimally oxidized  $c$ -axis oriented thin film (sample *H1*) grown on a SrTiO<sub>3</sub> substrate. The free face of the substrate was fastened using vacuum grease in a flowing-He-gas cryostat so that the ( $ab$ ) plane was lying in the holder plane. We used a multi-channel triple subtractive Jobin-Yvon T64000 spectrometer equipped with a charge-coupled device (CCD) detector. Bandpass filters were placed on the incident beam path. The sample was excited with the 676.4 nm (1.83 eV) laser line in off-resonant condition, with a power density less than 1 MW/m<sup>2</sup>. One of the advantages of working with this red line is that we have been able to considerably increase the resolution  $S$  of the experiment ( $\approx$  by a factor 2). With slits opened to 40  $\mu$ m,  $S$  was 1.15 cm<sup>-1</sup> for  $\lambda_L=514.5$  nm and 0.6 cm<sup>-1</sup> for  $\lambda_L=676.4$  nm. Moreover, remnant spurious plasma lines at 15, 42, 63, 67, 93, 105, 140, 165, 177, 229, 300, and 382 cm<sup>-1</sup> did not interfere in any way with the sample signal. A satisfactory signal to noise ratio was obtained by setting the spectral resolution  $\leq 2$  cm<sup>-1</sup>. A 90° scattering geometry was chosen: the laser beam was focused at grazing incidence  $\theta_p$  near the Brewster angle, i.e.,  $70^\circ < \theta_p < 80^\circ$ . We define the laboratory axes by  $x$ ,  $y$ , and  $z$ . The light was then collected along the direction  $y$  making a small angle ( $\approx 20^\circ$ ) with the  $c$ -axis direction of the crystal. The polarizations of the incident and scattered light were therefore denoted in the following by  $YY$  and  $YX$  with  $X$  and  $Y$  lying almost along the directions  $[100]$  and  $[010]$ . The corresponding Porto notations are  $y(YY)x$  and  $y(YX)x$ .

Experiments concerning the variation of oxygen ordering were carried out at room temperature with a 100 $\times$  microscope objective using the 514.5 nm (2.4 eV) laser line. We studied the backscattering from various  $a$ - and  $c$ -axis films with  $S=4-5$  cm<sup>-1</sup>. The laser beam and the scattered light were directed along  $z$  and polarized along  $X$  and  $Y$  directions in the plane of the films. The polarization are  $z(YY)z$  when both incident  $\mathbf{e}_i$  and scattered  $\mathbf{e}_s$  fields are parallel ( $\parallel$  notation) and  $z(YX)z$  for crossed field directions ( $\perp$  notation). Possible loss of oxygen in the samples due to laser heating is carefully examined in the following section.

### C. Laser heating effects

On performing Raman experiments, special attention should be paid to the effects of laser heating, which in the

case of YBCO-type materials may lead to oxygen loss (or in-diffusion, depending on the ambient atmosphere) and disorder in the oxygen positions. We will estimate the increase of the temperature of our films, during measurements, using the heat model of Bock,<sup>20</sup> which proved to be fairly consistent with experimental measurements. In our case the following inequality holds:  $h \leq r_e \ll d$ , where  $h$  is the thickness of the film,  $r_e$  is the effective radius of the laser spot, and  $d$  is the thickness of the substrate. Retaining only significant terms we rewrite the formula in the following form:

$$\Delta_{\text{total}} = \Delta_{\text{bd}} + \Delta_{\text{sub}}, \quad (1)$$

where  $\Delta_{\text{bd}}$  is the temperature jump across the film-substrate boundary, which is due to the thermal resistance  $\rho_{\text{bd}}$  of the interface:

$$\Delta_{\text{bd}} = \rho_{\text{bd}} \frac{(1-R)P}{\pi r_e^2} [1 - \exp(-h/l)]. \quad (2)$$

The term

$$\Delta_{\text{sub}} = \frac{(1-R)P}{2k_{\text{sub}}r_e\sqrt{\pi}} [1 - \exp(-h/l)] \quad (3)$$

expresses the temperature rise across the depth of the substrate (the temperature of the substrate holder is assumed to be unaffected by the laser heating, and equal to the ambient temperature).  $\Delta_{\text{tot}}$  is thus the total temperature difference between the film and the substrate holder. Notations are the following:  $R$  is the reflectance of the film surface,  $P$  is the incident laser power,  $l$  is the penetration depth for light in the material of the film, and  $k_{\text{sub}}$  is the thermal conductivity of the substrate. For  $R$ ,  $l$ , as well as for  $k_{\text{sub}}$  at different temperatures, we take values cited in the work of Bock.<sup>20</sup> For the measurements at room temperature we used an incident laser power  $P$  of 4–5 mW, focused on a spot of  $\approx 5$   $\mu$ m diameter. The calculated value for  $\Delta_{\text{tot}}$  is about 30 K in the case of a SrTiO<sub>3</sub> substrate and 18 K in the case of a MgO substrate. Thus, in every case the temperature of the film during measurements did not exceed 60 °C, and no oxygen depletion or disordering due to heating may be expected.

At low-temperature measurements  $P$  varied between 10 and 20 mW, but the diameter of the spot was considerably larger  $\approx 100$   $\mu$ m than for micro-Raman measurements. Calculations show that under these conditions, the difference between the actual temperature of the film and the temperature of the holder measured during the experiment is no more than 1–2 K. Therefore, in this paper, we will not distinguish between the measured temperature and the actual sample temperature.

## III. THE MODEL OF INTERACTION BETWEEN A CONTINUUM AND TWO PHONONS

### A. Model Hamiltonian

In his pioneering work<sup>21</sup> Fano has considered the case of interaction between a number of discrete states and a common excitation continuum. His approach is based on solving the eigenvalue problem in the energetic representation of the unperturbed Hamiltonian. It implies that the self-energy of the discrete states, which is due to the interaction with exci-

tation different from that in the continuum, is disregarded. Since in our case this self-energy turned out to be comparable or greater than the linewidth induced by the interaction with the continuum, and for the purpose of the computational convenience we will choose another way, based on the evaluation of the Green's function of the system.

We consider two oscillators of bare frequencies  $\Omega_a$  and  $\Omega_b$ , and masses  $M_a$  and  $M_b$  presenting, respectively, pure symmetric vibrations of Ba and Cu(2) (plane copper) atoms. We also consider a quasicontinuum, which consists of a large number of discrete excited states  $|n\rangle$  with energies  $E_n$ . At the final stage we will perform a transition to the limit of a real continuum, introducing the density of states

$$\rho(E) = -\frac{1}{\pi} \text{Im} \sum_n \frac{1}{E - E_n + i0} \quad (4)$$

and its Hilbert transform

$$R(E) = \text{PV} \int \frac{\rho(E')}{E - E'} dE'. \quad (5)$$

We choose the Hamiltonian of the system in the following form

$$\begin{aligned} \hat{H} = & \frac{\hat{P}_a^2}{2M_a} + \frac{M_a \Omega_a^2}{2} \hat{Q}_a^2 + \frac{\hat{P}_b^2}{2M_b} + \frac{M_b \Omega_b^2}{2} \hat{Q}_b^2 + \sum_n E_n |n\rangle \langle n| \\ & + (g_a \hat{Q}_a + g_b \hat{Q}_b) \sum_n (|n\rangle \langle \text{GS}| + \text{H.c.}). \end{aligned} \quad (6)$$

The last term represents the oscillator-continuum interaction,  $g_a$  and  $g_b$  being the strengths (assumed to be real) of the deformation potentials created by the oscillators, and  $|\text{GS}\rangle$  denotes the ground state of the system.

We assume that the excitations from the continuum lie in the energetic interval, which overlaps the energies of the one-phonon excitations,  $\hbar\Omega_a$  and  $\hbar\Omega_b$ . Due to nearly resonant conditions, it will be much more probable for a one-phonon state to evolve into a single excitation from the continuum lying in the small vicinity of  $\hbar\Omega$ , than to be transformed into a two-phonon state plus one excitation from the continuum [these are the two first-order processes generated by the interaction part of the Hamiltonian (6)]. This allows us to restrict the subspace of the states excited in the Raman process to those generated by the basis of all states  $|n\rangle$  plus one-phonon excited states  $|a\rangle$  and  $|b\rangle$  of the oscillators. In this basis the matrix elements of the Hamiltonian are the following:

$$E_a = H_{aa} = \langle a | \hat{H} | a \rangle = \hbar\Omega_a, \quad (7)$$

$$E_b = H_{bb} = \langle b | \hat{H} | b \rangle = \hbar\Omega_b, \quad (8)$$

$$H_{ab} = \langle a | \hat{H} | b \rangle = 0, \quad (9)$$

$$H_{a(b)n} = \langle a(b) | \hat{H} | n \rangle = V_{a(b)} = g_{a(b)} \sqrt{\frac{\hbar}{2M_{a(b)}\Omega_{a(b)}}}, \quad (10)$$

$$H_{nm} = \langle n | \hat{H} | m \rangle = E_n \delta_{nm}. \quad (11)$$

## B. Raman intensity

We assume that the oscillators and the excited states from the continuum are allowed to scatter light. If we denote the frequency shift in the scattering process for the incident photon of circular frequency  $\omega_i$  by  $\omega$ , the differential cross section for the Stokes process is given by

$$\begin{aligned} \frac{d^2\sigma}{d\Omega d\omega} = & -\frac{1}{\pi} [1 + n(\omega)] (\omega_i - \omega)^2 \\ & \times \langle \text{GS} | \hat{T}^+ \text{Im} \hat{G}(\omega + i0) \hat{T} | \text{GS} \rangle, \end{aligned} \quad (12)$$

where  $\hat{T}$  is a properly chosen transition operator,  $n(\omega)$  is the Bose factor, and

$$\hat{G}(\omega) = (\hbar\omega - \hat{H})^{-1} \quad (13)$$

is the Green's function (propagator) of the Hamiltonian.

The matrix elements of  $\hat{T}$  between the ground state and the excited states from the basis will be denoted by  $T_a$ ,  $T_b$ , and  $T_n$ , respectively, and further will be assumed to be real numbers. We also will assume that all states from the continuum have the same scattering amplitudes  $T_n = T_{\text{cont}}$ . If this condition is satisfied, it is straightforward to show that the problem for calculation of the Raman intensity (12) is reduced to the effective three-state problem

$$\frac{d^2\sigma}{d\Omega d\omega} = -\frac{1}{\pi} [1 + n(\omega)] (\omega_i - \omega)^2 T^+ \text{Im} G(\omega + i0) T. \quad (14)$$

$T$  is a vector column, containing the matrix elements  $T_a$ ,  $T_b$ , and  $T_{\text{cont}}$ , and  $G$  is a reduced Green's function  $3 \times 3$  matrix, given by the equation

$$\begin{aligned} \mathbf{G}^{-1}(\omega + i0) = & \begin{pmatrix} \hbar\omega - E_a + i0 & 0 & V_a \\ 0 & \hbar\omega - E_b + i0 & V_b \\ V_a & V_b & \frac{1}{R - i\pi\rho} \end{pmatrix}. \end{aligned} \quad (15)$$

Equation (15) implies that the interaction of the two oscillators with the continuum may be represented as an effective interaction with a single overdamped excited state.  $R$  and  $\rho$ , as defined in Eqs. (4) and (5) depend on  $\omega$ . It would be reasonable from a physical point of view to take some flexible spectral shape for  $\rho$ , e.g., linear or quadratic. However, our experience showed that for an increasing number of adjustable parameters, which describe the continuum, we are compelled to pay by lowering the accuracy of the fit. Since the goal of this section is to establish the fact that the Cu(2),  $A_g$  vibrations interact with the continuum, we will adopt a simplified assumption that  $\rho \approx \text{const}$  and  $R \approx 0$  in the spectral range of interest. To account for the broadening of one-phonon states, induced by anharmonic coupling with other vibrational branches, in the calculation of the scattering efficiency we will add a damping term to the one-phonon energies, which together with the bare frequencies will be determined by fit to the experimental spectra:

$$E_{a(b)} \mapsto E_{a(b)} - i\Gamma_{a(b)}. \quad (16)$$

It should be stressed that there is an intrinsic ambiguity in the determination of the parameters, which enter the right-hand side of Eq. (15), when fitting the Raman intensities. It is due to the fact that the intensity, calculated by means of formula (14) is invariant with respect to the following scaling transformation ( $\lambda$  is an arbitrary real number):

$$\rho \mapsto \lambda^2 \rho, \quad (17)$$

$$R \mapsto \lambda^2 R, \quad (18)$$

$$V \mapsto V/\lambda, \quad (19)$$

$$T_{\text{cont}} \mapsto T_{\text{cont}}/\lambda. \quad (20)$$

For this reason we may arbitrarily fix the value of one of the parameters (20) and optimize the calculated intensity with respect to the scaling invariant combinations. For the same arguments, the only relative sign of  $T_{\text{cont}}$  and  $V$  may be determined. We will set  $\rho = 1/\pi$  and  $V_a > 0$ , and will fit with respect to the following scaling invariant quantities:

$$v_{a(b)} = V_{a(b)} \sqrt{\pi \rho}, \quad (21)$$

$$t_{a(b)} = T_{a(b)} / (T_{\text{cont}} \sqrt{\pi \rho}), \quad (22)$$

$$r = R / (\pi \rho), \quad (23)$$

$$I_0 = K \rho T_{\text{cont}}^2. \quad (24)$$

$I_0$  is the scattering intensity which is due only to the excitations from the continuum, and which would be measured if there was no interaction between the oscillators and the continuum. The constant  $K$ , introduced in the last equation, accounts for the fact that we do not perform measurements of the absolute Raman intensities, but of phonon counts which depend on the sensitivity of the detector and the details of the experimental setup. For convenience, we further set  $\hbar = 1$ , and for energy and frequency we choose the same unit of measure,  $\text{cm}^{-1}$ .

#### IV. TEMPERATURE DEPENDENCE AND FINE STRUCTURE OF THE Ba AND Cu BANDS

##### A. Application of the interference model to Ba and Cu lines

The spectra of two thin films, *H1* and *Y6*, were chosen to test the interference model presented in Sec. III. Both samples presented satisfactory electrophysical parameters ( $T_c = 91$  K,  $\Delta T = 1$  K and  $T_c = 85$  K,  $\Delta T = 4$  K, respectively) and were therefore assumed to be nearly optimally doped as indicated by the apex oxygen frequency at  $\approx 500$   $\text{cm}^{-1}$ . Additional low-frequency lines were found in sample *H1* at 184, 213, 229, 262  $\text{cm}^{-1}$  as well as a weak bump line near 580  $\text{cm}^{-1}$  suggesting some inhomogeneity in the oxygen sublattice<sup>22–24</sup> whereas the spectrum of *Y6* was characteristic of a sample free of defects. Figure 1(a) presents the low-frequency Raman spectra taken from sample *H1* at different temperatures. The best fit to the experimental data was obtained, when to the intensity, calculated by means of the two-oscillator–and–continuum model (14), were added contributions of two Lorentzians and a relatively weak incoherent linear background. For clarity, the three main additive

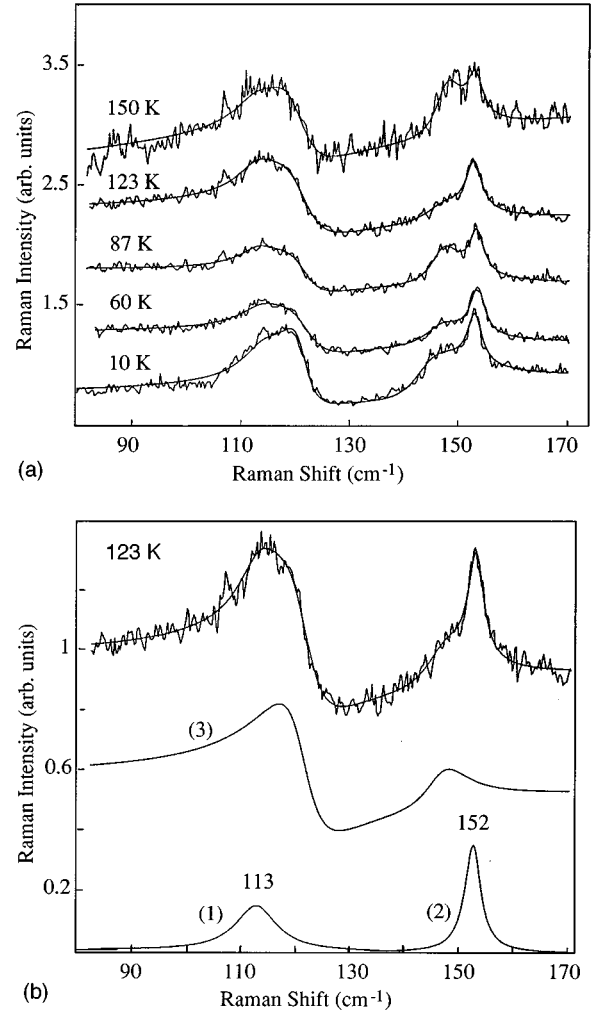


FIG. 1. (a) Raman spectra taken from an optimally oxygenated film of  $\text{YBa}_2\text{Cu}_3\text{O}_{6+\delta}$  at different temperatures (sample *H1*), and theoretical fits based on the model described in Sec. III. The spectra are shifted vertically for convenience. (b) Different additive contributions to the fitted line shape at  $T = 123$  K: lines (1) and (2) are Lorentzians, and the profile (3) is obtained in the model of the two oscillators interacting with common continuum.  $y(YY)x$  polarization.

contributions to the Raman intensity are also shown in Fig. 1(b). Adjusted values for the bare frequencies of the interacting oscillators were found to be  $\Omega_a = 119$  and  $\Omega_b = 146$   $\text{cm}^{-1}$ , and for frequencies of the two additional peaks  $\Omega'_a = 113$  and  $\Omega'_b = 152$   $\text{cm}^{-1}$ . Deviations from these values at different temperatures are irregular, and lie within  $\pm 1$   $\text{cm}^{-1}$  which is comparable to the frequency resolution of the spectrometer.

Fitted values for the oscillator-continuum interactions are summarized in Table II. In parentheses are shown estimated confidential intervals, obtained in the fitting procedure. Although at high temperatures the magnitude of the interaction between the 146  $\text{cm}^{-1}$  mode and the continuum is 4–5 times smaller than the corresponding one for the 119  $\text{cm}^{-1}$  mode, the confidential interval never crosses the zero. Changes of the interaction parameter  $v_a$  with the temperature are of the order of the accuracy of the fit. However, for the Cu(2) mode, some tendency for increasing  $v_b$  at low temperatures

TABLE II. Fitted values of the interaction parameters  $v_a$  and  $v_b$  at different temperatures. Estimated confidential intervals are given in parentheses.

$T$ (K)	$v_a$ (cm <sup>1/2</sup> )	$v_b$ (cm <sup>1/2</sup> )
10	0.77(± 0.06)	0.79(± 0.1)
60	0.97(± 0.06)	0.28(± 0.07)
87	0.88(± 0.07)	0.19(± 0.06)
123	0.93(± 0.05)	0.20(± 0.08)
150	0.81(± 0.11)	0.19(± 0.10)

may be traced. For comparison, Fig. 2(a) presents the best fit to the experimental data at 10 K, obtained in the assumption that *only* the Ba mode interacts with the continuum. It is apparent that this fit misses to reproduce some important details of the real spectral shape, and demonstrates that the coupling of the Ba and Cu(2) modes with a *common continuum* is a relevant model especially at low temperatures.

The temperature variation of  $v_b$  makes possible the interpretation of the scattering continuum as being composed by

low-energy interband transitions. The rise of the temperature increases the electronic occupation of the upper band, which reduces the density of the allowed transitions. In the work of Bogachev *et al.*<sup>13</sup> it was proposed that the continuum which interacts with Ba vibrations is due to transitions from the lower, predominantly O(4)  $p_x$  band to the upper, predominantly O(4)  $p_y$  band in the vicinity of the *SR* line [ $\mathbf{k} = (\pi/a, \pi/b, \xi)$ ] of the Brillouin zone. This hypothesis is consistent with our observation in two aspects. It separates in the real space the states which form the continuum from the conducting CuO<sub>2</sub> planes, and leaves them unaffected by the superconducting transition. In the tetragonal semiconducting phase,  $p_x$  and  $p_y$  bands coincide in energy due to the tetragonal symmetry and thereby Ba line asymmetry should disappear, as observed experimentally. However some objections against this scenario may be drawn. As shown by first-principles band structure calculations for YBa<sub>2</sub>Cu<sub>3</sub>O<sub>7</sub>,<sup>25</sup> the two bands have some admixture with the Ba and Cu(1) orbitals, but not with the Cu(2) ones, and it is doubtful that Cu(2) vibrations can couple to these transitions, as our experiments show. Also, the point group symmetry of the wave vector along the *SR* line is  $C_{2v}$ , and the wave functions composed by the  $p_x$  and  $p_y$  orbitals transform according to the  $B_1$  and  $B_2$  irreducible representations, respectively. It means that the transitions between the two bands are Raman inactive in *XX* and *YY* scattering configurations along the *SR* line, where the spectral maximum of the transitions is located.

Another possible explanation of our observations may be derived from the same work. It is shown that the chain electronic band crosses near the Fermi level the odd plane band (with respect to the horizontal mirror containing the Y atom) at the point  $[0.5(\pi/a), 0.2(\pi/b), 0]$ . Transitions between these two bands give rise to a flat feature in  $\epsilon''(\omega)$  between 0 and 200 cm<sup>-1</sup>, just in the spectral range, where the two phonons lie. There are no symmetry restrictions on the *XX* and *YY* Raman transition amplitudes, and moreover Cu(2) vibrations may effectively modulate the states from the plane band. Difficulties, however, arise when one attempts to explain the invariance of the phonon-continuum interference upon opening of a large superconducting gap. This obstacle may be avoided if one assumes that the superconducting gap is strongly anisotropic, as suggested in a large number of works on the high-temperature superconductors. Then the gap at  $\mathbf{k} = [0.5(\pi/a), 0.2(\pi/b), 0]$  may have a value less than the energy of the Ba phonon ( $2\Delta < 120$  cm<sup>-1</sup>), and the two phonons will lie in the interval of nonzero electronic density of states. If it does take place, it is possible to expect that opening of the gap will transfer electronic spectral density to higher energies, thus increasing at low temperatures values of the parameters  $v_a$  and  $v_b$ . It is interesting to note that Monien *et al.*<sup>26</sup> have come to the conclusion of the existence of an anisotropic gap, from considerations of the continuum which interacts with the out-of-phase O(2)-O(3) mode at 330 cm<sup>-1</sup>.

Interaction of the Ba and Cu vibrations with a common continuum of low-energy electronic excitations may at least qualitatively explain why *ab initio* calculations<sup>17,18</sup> overestimate the degree of Ba-Cu mixing in the modes at 119 and 146 cm<sup>-1</sup>. In fact first-principles lattice dynamical calculations are based on the adiabatic, frozen-phonon approach. It

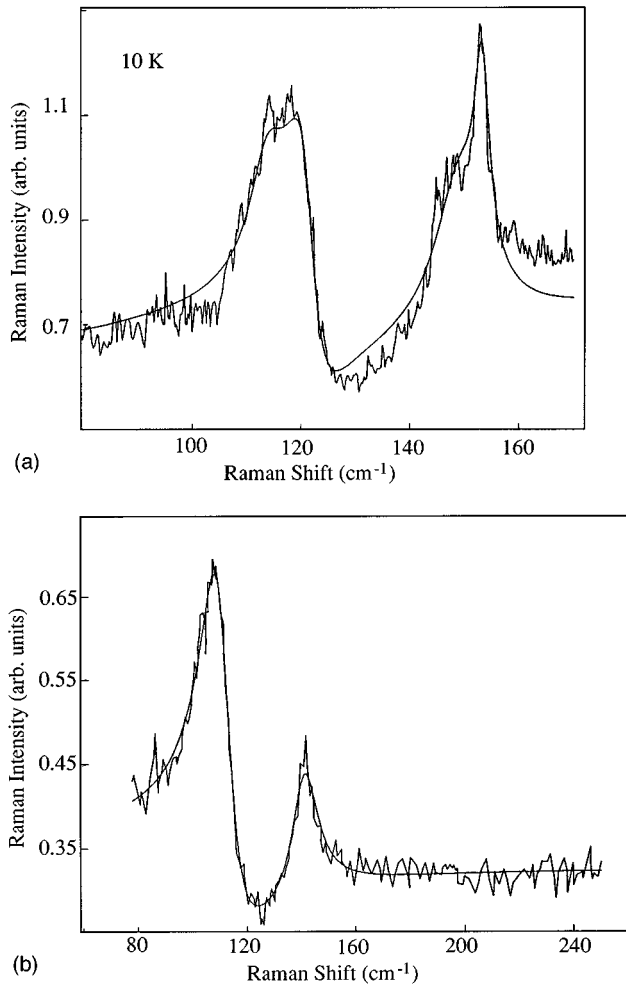


FIG. 2. (a) Fit to the spectrum of Fig. 1, obtained in the assumption that only Ba vibrations interact with the continuum. (b) Raman spectrum of an optimally oxygenated thin film of YBa<sub>2</sub>Cu<sub>3</sub>O<sub>6+ $\delta$</sub>  at 293 K (sample Y6), and the theoretical fit to it.  $y(YY)x$  polarization.

is straightforward to show on the basis of the model Hamiltonian (6) that in the frozen-phonon picture, an off-diagonal element of the dynamical matrix appears, which is equal to  $-2g_a g_b R(0)$ , where  $R(0)$  is the Hilbert transform of the density of electronic transitions at zero energy. It implies that in the adiabatic approximation all electronic transitions give contribution with the same sign to the off-diagonal dynamical matrix element. The actual mixing of the Ba and Cu displacements in the mode of frequency  $\Omega$  is, however, determined by  $-2g_a g_b R(\hbar\Omega)$ . If  $\hbar\Omega$  is within the excitation continuum, the electronic transitions from below and above this value will give contributions with opposite sign, which will partially compensate each other, thus leading to mode mixing which is lower than predicted on the basis of the frozen-phonon picture. Note also that in the same approximation there are *negative* diagonal contributions to the dynamical matrix equal to  $-2g_a^2 R(0)$  and  $-2g_b^2 R(0)$ . They will lead to *underestimated* values for the normal mode frequencies in the frozen-phonon calculations. Indeed LAPW calculations give 105 and 127  $\text{cm}^{-1}$  for the 119 and 146  $\text{cm}^{-1}$  modes, respectively.<sup>18</sup>

Recently multimode behavior has been observed for the apex  $A_g$  band at 480–500  $\text{cm}^{-1}$  on oxygen off-stoichiometric samples of the  $R\text{Ba}_2\text{Cu}_3\text{O}_{6+\delta}$  family.<sup>22–24</sup> It is usually ascribed to separation of the basal plane oxygen atoms into two or three types of ordered domains with different oxygen content, which give additive contributions to two or three shifted Lorentzian lines. The two additional Lorentzian lines which appear in our spectra at 113 and 152  $\text{cm}^{-1}$  may stem from oxygen-deficient regions which coexist with orthorhombic surrounding of high oxygen content. If these oxygen-deficient regions are of semiconducting phase, then all low-energy band transitions should disappear, and Ba and Cu vibrations will give two incoherent Lorentzian contributions to the spectrum. Concerning the Raman activity of our samples, it is easy to show that the predicted vibrational modes for  $\text{YBa}_2\text{Cu}_3\text{O}_6$  ( $D_{4h}$  point group) and  $\text{YBa}_2\text{Cu}_3\text{O}_7$  ( $D_{2h}$ ) are represented, respectively, by

$$\Gamma_{\text{tetra}} = 4A_{1g} + B_{1g} + 5E_g + 5A_{2u} + B_{2u} + 6E_u$$

and

$$\Gamma_{\text{orthoI}} = 5A_g + 5B_{2g} + 5B_{3g} + 7B_{1u} + 7B_{2u} + 7B_{3u}.$$

If one supposes that we have coexistence of the ortho-I and ortho-II phases in our sample, the vibrational modes for the supercell  $\text{Y}_2\text{Ba}_4\text{Cu}_6\text{O}_{13}$  are given by  $\Gamma_{\text{orthoII}} = 11A_g + 3B_{1g} + 11B_{2g} + 8B_{3g} + 2A_u + 13B_{1u} + 11B_{2u} + 13B_{3u}$ .

The number of modes in this oxygen-deficient supercell is twice that of the fully oxidized phase and one should expect a splitting of some lines. Additional Raman modes have to be allowed in the spectrum. We believe that the two components of the Ba mode may be linked to two phases with different oxygen contents. These could be the ortho-I and ortho-II phases. The former can be identified by the highest frequency component since the latter was ascertained by previous workers to appear at 113–114  $\text{cm}^{-1}$ . These phases would form domains with different scattering probabilities varying vs temperature in different channels. This effect would consequently lead to a variation of the intensities of both components and cause different interactions with

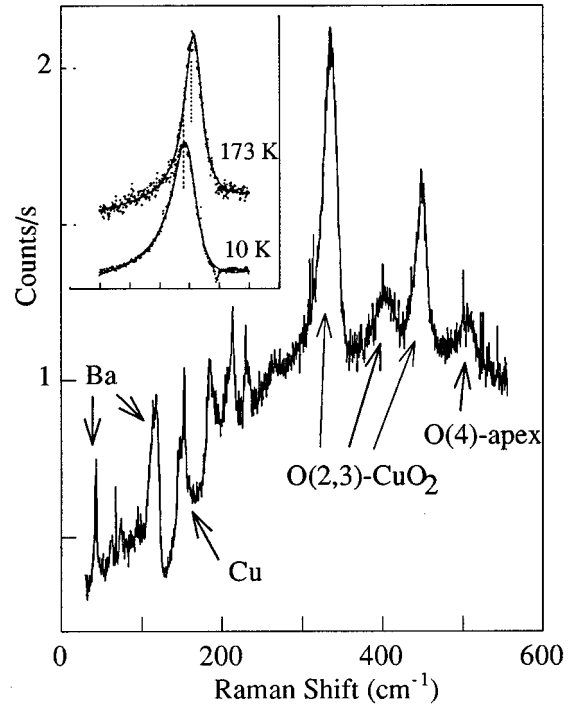


FIG. 3. Raman spectrum of film *H1* recorded in  $y(YY)x$  polarization with  $\lambda_L = 676.4$  nm. In the inset, the line shapes of the  $B_{1g}$  mode taken at 173 K and 10 K show strong softening and broadening below  $T_c$ . Solid lines indicate a Fano fit.

the electronic scattering. To prove this suggestion we present the spectrum from sample *Y6*. As seen from Fig. 2(b) there is no trace of the two additional Lorentzians, and the overall shape of the spectrum may be perfectly described within the model of two oscillators interacting with the common continuum. This observation fits well with the fact that the sample *Y6* displays no features of oxygen inhomogeneity and disorder. Obtained parameters (at 293 K) are similar to those of the previously studied sample:  $\Omega_a = 119(\pm 1)$   $\text{cm}^{-1}$ ,  $\Omega_b = 146(\pm 1)$   $\text{cm}^{-1}$ ,  $v_a = 1.0(\pm 0.1)$   $\text{cm}^{1/2}$ ,  $v_b = 0.12(\pm 0.08)$   $\text{cm}^{1/2}$ .

### B. Behavior of the $B_{1g}$ mode

In Fig. 3 we have plotted the whole spectrum of film *H1* obtained at 10 K for  $\lambda_L = 676.4$  nm. Fano line shapes are observed for almost all modes in the whole temperature range. The inset shows the Raman line shapes of the  $B_{1g}$ -like O(2) mode at  $\approx 335$   $\text{cm}^{-1}$  recorded at 10 K and 173 K. We note that above  $T_c$  the asymmetry is much weaker than in the superconducting state. The spectra shows considerable changes in frequency, intensity, and linewidth when going below  $T_c$ . This line may be fitted for all temperatures with a Fano function:

$$F(\omega) = \frac{(\omega - \omega_p + \Gamma/s)^2}{(\omega - \omega_p)^2 + \Gamma^2} + a\omega + b, \quad (25)$$

where  $\omega_p$  and  $\Gamma$  are, respectively, the frequency and the half width at half maximum (HWHM) of the bare phonon, and  $s = 1/q$  is a dimensionless asymmetry parameter affecting the line shape. The linear term accounts for the spectral back-

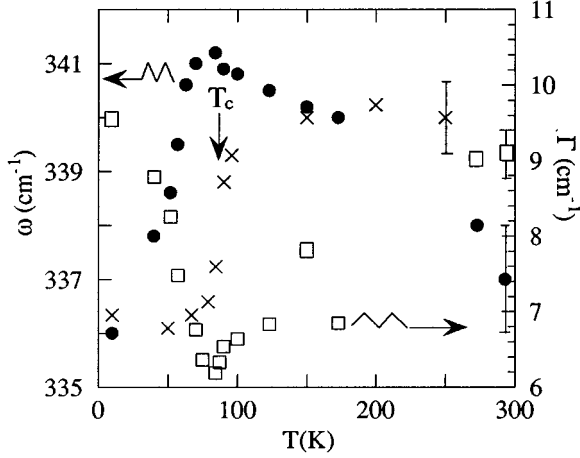


FIG. 4. Anomalous  $B_{1g}$  oxygen phonon from sample  $H1$ . Variation of maximum-intensity frequency  $\omega_p + \Gamma/q$  (dots) and linewidth (squares). The crosses indicate the frequencies at  $\mathbf{q} = (0.2, 0, 0)$  measured by Pyka *et al.* with inelastic neutron scattering for a single crystal. In  $\text{cm}^{-1}$  units.  $\lambda_L = 676.4$  nm.

ground. The respective Fano parameters for 10 K and 173 K are  $q = -4.7$  and  $-11$ ,  $\Gamma = 9.5$  and  $6.8 \text{ cm}^{-1}$ ,  $\omega_p = 338.8$  and  $340.6 \text{ cm}^{-1}$ . It should be emphasized that the asymmetry factor  $q$  for the red line excitation is close to that obtained in the spectra excited by the  $\lambda_L = 514.5$  nm laser line ( $q = -4.3$ ). Taking into account that

$$q = \frac{T_{\text{phonon}}}{T_{\text{cont}}} \frac{V}{\Gamma}, \quad (26)$$

where  $T_{\text{phonon}}$  and  $T_{\text{cont}}$  are the matrix elements of the vibrational and electronic transitions, and  $V$  is the deformation potential, the scattering continuum has the same resonant behavior as that of the  $335 \text{ cm}^{-1}$  phonon. This observation has not been mentioned previously.

The overall temperature dependence of the line shape of the  $B_{1g}$  oxygen phonon is depicted in Fig. 4. The most interesting result is that the vibrational frequency of this phonon softens in the superconducting state by about  $5\text{--}6 \text{ cm}^{-1}$  for  $\lambda_L = 676.4$  nm. The onset of the anomalies occur near  $T_c$ . This is consistent with superconductivity originating in the  $\text{CuO}_2$  planes and involving optical phonons, and not necessarily acoustic phonons. The energy of the  $B_{1g}$  phonon is probably below the gap energy  $2\Delta(0)$ . Thus the behavior of this mode is an indication that the lower limit of the superconducting gap energy is near  $40 \text{ meV}$  ( $335 \text{ cm}^{-1}$ ). This yields  $2\Delta/kT_c \geq 5.3$ , i.e., a strong electron-phonon coupling in a BCS-type mechanism. A confirmation of the low-frequency shift of this mode below  $T_c$  was firmly established by inelastic neutron scattering in  $\text{O}_{6.92}$  and  $\text{O}_7$  single crystals as well as its dependence against  $\delta$ .<sup>27</sup>

## V. OXYGEN SUBLATTICE ORDERING

### A. Apex $A_g$ mode

According to several authors the apex oxygen frequency of  $\text{Y}(\text{Pr})\text{Ba}_2\text{Cu}_3\text{O}_{6+\delta}$  depends on the oxygen content  $x$  and

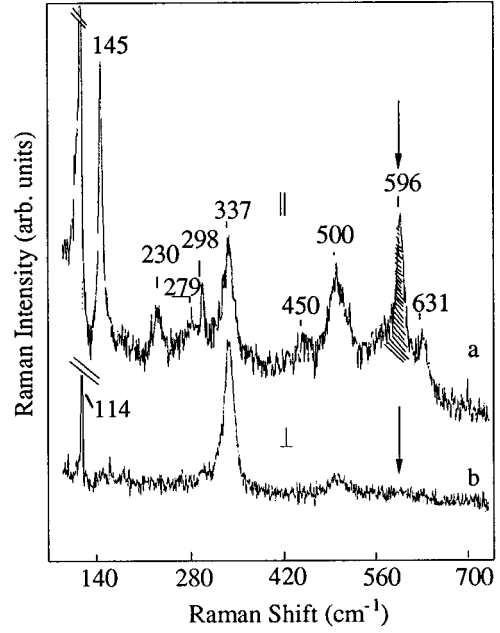


FIG. 5. Backscattering micro-Raman spectra of a  $c$ -axis oriented  $\text{YBa}_{1.93}\text{Cu}_{2.9}$  thin film optimally oxygenated (sample  $Y6$ ,  $T_{\text{onset}} = 89 \text{ K}$ ,  $\Delta T = 4 \text{ K}$ ,  $h = 1400 \text{ \AA}$ ) with weak oxygen disorder; (a)  $z(YY)z$  polarization ( $\parallel$ ), (b)  $z(YX)z$  polarization ( $\perp$ ).  $\mathbf{E}$  is in the  $(ab)$  plane which is the  $XY$  plane, the laser beam being directed along  $z$ .  $\lambda_L = 514.5$  nm,  $T = 293 \text{ K}$ . The defect-induced modes are dashed.

follows an empirical relationship with  $x \approx 0.037\omega_{\text{apex}} - 11.55$ .<sup>28</sup> Thus, an  $\omega_{\text{apex}}$  of  $500 \text{ cm}^{-1}$  should characterize an optimally oxygenated sample. This property originates from the variation of the  $c$ -cell parameter with  $\delta$ . This  $A_g$  mode comes from a symmetric out-of-plane motion of the  $\text{O}(4)$  atoms. There is a contraction of the unit cell when  $x = 6 + \delta$  increases and the frequency of the apex  $A_g$  mode raises slightly due to Cu-O bond hardening. An interesting observation made in the present work was that in  $c\perp$ -oriented films, the  $B_{1g}$  mode at  $\approx 340 \text{ cm}^{-1}$  is always considerably enhanced with respect to the  $500 \text{ cm}^{-1}$  mode. Conversely, in the case of  $a\perp$  orientation the apex oxygen mode is the dominant one in the Raman spectrum. In a preliminary analysis, these characteristic intensity enhancements in the Raman spectra provide a way for quick identification of the deposition conditions of thin films without running the sample in XRD.

### B. Additional Raman lines

In this section we examine the additional modes of the oxygen sublattice in the spectra of  $c$ - and  $a$ -axis thin films recorded at room temperature. Consider the spectra in Fig. 5 taken from a thin  $c$ -axis oriented film with good superconducting properties. The  $z(YY)z$  ( $\mathbf{e}_i \parallel \mathbf{e}_s$ ) polarized Raman spectrum exhibits intense lines at  $145, 337, 500 \text{ cm}^{-1}$  in addition with lines at  $230, 279, 298, 596,$  and  $632 \text{ cm}^{-1}$ . We note that in the perpendicular  $z(YX)z$  polarization ( $\mathbf{e}_i \perp \mathbf{e}_s$ ) the  $337 \text{ cm}^{-1}$  line persists in the spectrum. We verify that this mode has a  $B_{1g}$ -like character due to the fact that the approximate symmetry of the superconducting phase is  $D_{4h}$

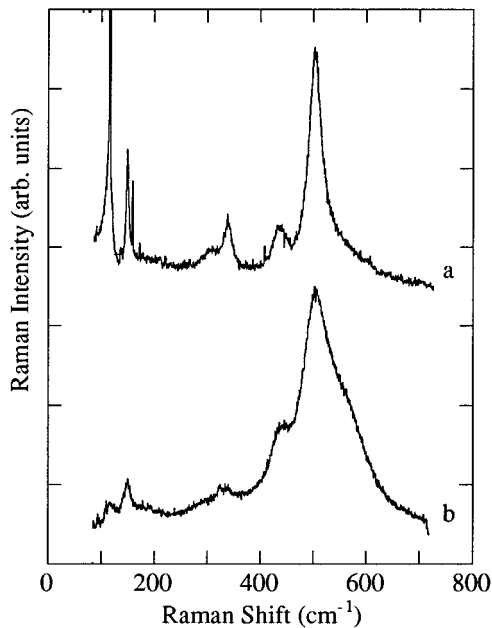


FIG. 6. Micro-Raman spectra of two  $a$ -axis films:  $H2$  (a) and  $H3$  (b). Note the strong intensity of the apex mode with respect to the conducting plane mode. The broad profile of the apex mode is obvious. In spectrum (b) ( $H3$ ) this profile is broadened by an additional spectral component. The line shape decomposition of this spectrum can be performed using Lorentzian functions with the following  $\omega$  and  $2\Gamma$  parameters (in  $\text{cm}^{-1}$ ): (434, 47.8), (504, 61), (562, 80.3).  $\lambda_L = 514.5$  nm,  $T = 293$  K.

since the film  $H1$  has very close  $a$  and  $b$  lattice parameters, with a  $c$  parameter of  $11.73$  Å. Separation of this mode from the other  $A_g$  modes is possible if the grains of the film are rotated at  $45^\circ$  with respect to the laboratory axes ( $X'$  and  $Y'$  directions).

Modes at (298) and  $631$   $\text{cm}^{-1}$  come likely from grains of the  $\text{CuO}$  precipitate. The other modes at 230, 279, and  $596$   $\text{cm}^{-1}$  may be compared to those found in deoxygenated and heated YBCO single crystals.<sup>29</sup> Indeed, with  $e_i$  parallel to the ( $ac$ ) crystalline edges, these spectra show strong modes at 596 and  $602$   $\text{cm}^{-1}$ . Their intensity is magnified when oxygen is depleted from the sample by thermal treatment, leading to the formation of the  $60$  K- $\text{O}_{6.5}$  ortho-II phase. Since secondary phases are not likely to grow within single crystals from such thermal processes it is tempting to ascribe these additional modes to a modification of the copper coordination possibly caused by oxygen vacancies and oxygen disorder. Note that the presence of lines at 270, 576, and  $590$   $\text{cm}^{-1}$  in  $\text{O}_{6.5}$  single crystals spectra has been confirmed by several workers.<sup>23,30,31</sup>

The behavior of these lines is well illustrated in Fig. 6 which compares two spectra of  $a$ -axis thin films grown on  $\text{MgO}$  substrates. The spectrum (a) is taken from a sample ( $H2$ ) with good superconducting properties ( $T_0 = 90$  K, transition width  $\Delta T = 11$  K). The curve (b) is from a metallic sample ( $H3$ ) with nonsatisfactory electrophysical parameters presenting a resistive tail with an actual  $T_c$  at 12 K and a large transition width  $\Delta T = 74$  K whereas the  $T_c$  at small but nonzero resistance is 77 K ( $T_{\text{onset}} = 86$  K). The apex-oxygen spectral region of this latter sample may be decom-

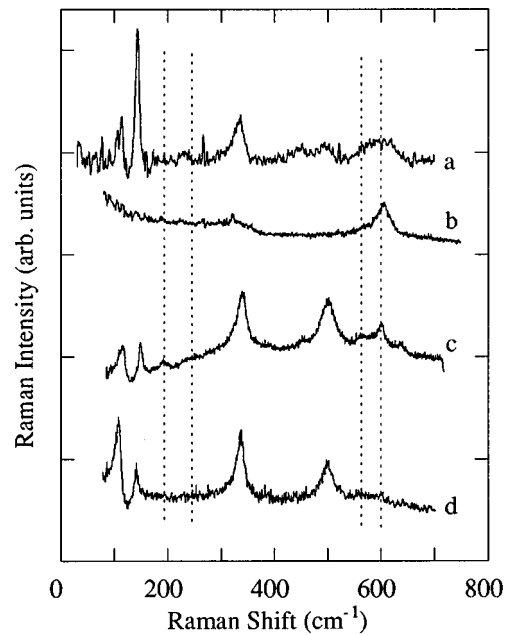


FIG. 7. Micro-Raman spectra of thin sputtered films obtained with different oxygen pressure ( $p_0$ ) and plasma pressure ( $p_T$ ) for  $z(Y,Y+X)z$  polarization. (a)  $p_T = 0.2$  Torr,  $p_0 = 0.008$  Torr, sample Y2. (b)  $p_T = 0.2$  Torr,  $p_0 = 0.105$  Torr, sample Y3. (c)  $p_T = 0.5$  Torr,  $p_0 = 0.1$  Torr, sample Y5. (d)  $p_T = 0.5$  Torr,  $p_0 = 0.125$  Torr, sample Y8.  $\lambda_L = 514.5$  nm,  $T = 293$  K. 1 Torr = 133 Pa.

posed into three Lorentzian functions extracted at  $434$   $\text{cm}^{-1}$  (oxygen of the  $\text{CuO}_2$  planes),  $504$   $\text{cm}^{-1}$  (apical oxygen), and at  $562$   $\text{cm}^{-1}$ . The HWHM of the  $504$   $\text{cm}^{-1}$  band is  $30.5$   $\text{cm}^{-1}$ , and is large compared to that of previous examples ( $\sim 15$   $\text{cm}^{-1}$ ). The electrophysical and Raman spectral parameters of this film show that it is presumably formed with grains of a small size which broaden this band. Indeed, in this case the sample area probed by the laser beam may have amorphous regions in which translational symmetry is broken so that long range order vanishes. Therefore the  $\mathbf{q} = 0$  selection rule is relaxed for such regions and phonons with all  $\mathbf{q}$  vectors are activated resulting in a tail from phonon density of states in the spectrum. Such effects were observed, for instance, in amorphous or microcrystalline semiconductors like silicon, Ge, or GaP.<sup>32</sup> It thus appears that there is a strong correlation between the relatively nonsatisfactory electrophysical parameters of film  $H3$ , its orientation ( $a \perp$ ), and the broad features of the Raman spectrum in the  $500$ – $600$   $\text{cm}^{-1}$  region. Furthermore, the apex mode position indicates that  $x = 6.9$  in this film.

### C. Influence of synthesis conditions on additional modes

Figure 7 displays the Raman spectra of samples synthesized at different oxygen pressure  $p_0$  within low or high total plasma pressure. The films obtained with a low total pressure exhibit broad bands between  $180$ – $300$   $\text{cm}^{-1}$  and  $500$ – $700$   $\text{cm}^{-1}$  whereas those obtained at high total pressure present narrow additional lines. There is a tendency that when the plasma pressure is high, an increase of  $p_0$  leads to a decrease in intensity of the modes at 190, 240, 560, 580, and  $600$   $\text{cm}^{-1}$ . When the plasma pressure is low these bands remain.

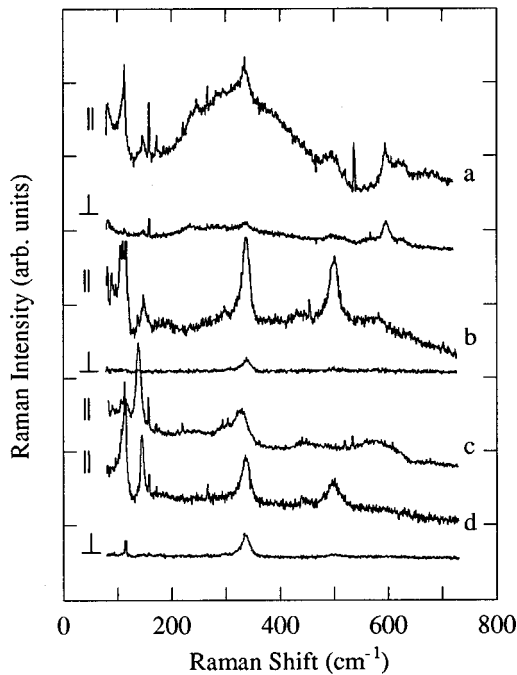


FIG. 8. Polarized micro-Raman spectra  $z(YY)z$  and  $z(YX)z$  from (a) sample Y4; (b) sample with properties similar to Y5; (c) sample Y1; (d) sample Y7.  $\lambda_L = 514.5$  nm,  $T = 293$  K.

This can be explained by the fact that at high plasma pressure the oxygen ions enter the chains at vacancies and then diminish the relative proportion of defects. We deduce that a high plasma pressure reduces the oxygen sublattice disorder considerably and this accounts for the excellent electrophysical values of the films. At low plasma pressure defects and vacancies persist in the structure although it was shown that no secondary phases were formed. We again observe that the Ba and Cu modes at 120 and 150  $\text{cm}^{-1}$  interact strongly as seen by the pronounced valley between these two modes.

Figure 8 compares the  $z(YY)z$  and  $z(YX)z$  polarized spectra of four different thin films synthesized with the same sputtering geometry. Common spectral features appear near 560 and 600  $\text{cm}^{-1}$  which are polarized like the  $A_g$  modes and yield no contribution [except for curve (a)] to the  $z(YX)z$  spectra. The strong depression in the scattering intensity is noticed in the spectral region between the Ba and Cu modes which supports our previous argument concerning the shape of the Ba mode and its mixing with the Cu mode.

In Fig. 9 we have plotted the Raman spectra of four  $\text{PrBa}_2\text{Cu}_3\text{O}_{6+\delta}$  insulating films. The apex mode frequency varies from 511 to 516  $\text{cm}^{-1}$  as a result of different oxygen stoichiometry. The relative intensities of the apex and conducting plane modes at 516 and 298  $\text{cm}^{-1}$  show that sample P7 has  $c\perp$  orientation whereas the others are  $a\perp$  films as checked with x-ray measurements. For all these samples, strong additional lines are seen again near 160, 170, 220, 560, and 596  $\text{cm}^{-1}$ . Those samples which have been synthesized with low oxygen pressure (P4, P7, P11) present the most intense additional lines.

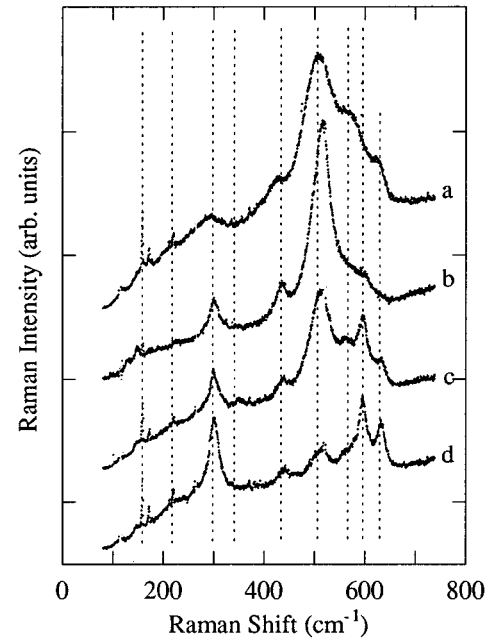


FIG. 9. Micro-Raman spectra of  $\text{PrBa}_2\text{Cu}_3\text{O}_{6+\delta}$  films: the Raman forbidden lines at 560 and 600  $\text{cm}^{-1}$  are particularly intense. (a) sample P4; (b) sample P10; (c) sample P11; (d) sample P7.  $\lambda_L = 514.5$  nm,  $T = 293$  K.

#### D. Origin of Raman-forbidden phonon modes

Our data reveal that oxygen disorder is not necessarily linked to oxygen depletion since the superconducting and insulating samples are optimally oxygenated (ortho-I phase) as indicated by the high apical oxygen frequency (between 500–504 and 511–516  $\text{cm}^{-1}$ ). Some of our Raman spectra simulate the spectra obtained on  $\text{O}_{6.5}$  oxygen-depleted ortho-II phase crystals cited by previous authors and one can suppose that in these films chain-oxygen disorder coexists with an average *macroscopic*  $\text{O}_7$  stoichiometry. This, we believe, is explained by the presence of *microphase domains* (of about 1000 to 2000 lattice constants since the laser spot size is about 2  $\mu\text{m}$ ). Raman spectroscopy is very sensitive to these domains where chain-oxygen atoms O(1) and O(5) are nonuniformly distributed.

Let us consider, as shown in the example given above, that several oxygen-depleted phases coexist with fully oxidized domains. From the previous normal modes analysis we get six in-plane O(2), O(3) modes for the ortho-I phase and four additional in-plane modes for the ortho-II phase. Some of the lines appearing at 230, 270, 560, and 590  $\text{cm}^{-1}$  could stem from in-plane motions in both structures. Since the frequency of these modes varies with the oxygen content present in the structure one could consider a connection with oxygen sublattice defects.

Moreover, as can be easily seen in the present spectra, these bands, which we can tentatively name “defect induced,” are more pronounced in those samples which show signatures of oxygen deficiency ( $T_c$  lower than the optimum value) or nonuniform distribution of the oxygen atoms (large  $\Delta T$ ). We now discuss several relevant experiments found in the literature which support our preliminary assumptions concerning the salient features of our Raman spectra.

We will first comment on the two bands at 230–240  $\text{cm}^{-1}$  and 595–600  $\text{cm}^{-1}$ . Thomsen *et al.*<sup>33</sup> have observed these two features on untwinned orthorhombic YBCO single crystals, and have established that they are intense in the *bb* scattering configurations. The authors have ascribed them to the Cu(1) and O(1) vibrations along the *Y* axis, activated in the Raman spectrum due to the presence of oxygen vacancies in the chains. This explanation is also supported by the fact that their crystal had a  $T_c$  lower than the optimal value of  $\approx 90$  K which indicates oxygen deficiency. Wake *et al.*<sup>34</sup> observed these modes on optimally oxygenated, untwinned samples under resonant conditions for the yellow excitation line of the Kr-ion laser ( $\lambda_L = 566$  nm). They also assigned them to the *b* axis vibrations of the Cu(1) and O(1) atoms, but attributed these excitations to a quadrupole-allowed transition to a virtual intermediate state. A strong band at 600  $\text{cm}^{-1}$  is also observed in high-temperature Raman experiments of Burns,<sup>29</sup> McCarty,<sup>35</sup> and Fantini,<sup>36</sup> and in turn it is identified as an infrared-active oxygen vibration, which is allowed to scatter light due to the oxygen disorder at high temperatures.

Finally, we would like to mention recent experiments of Ivanov and Iliev<sup>37</sup> on laser-assisted, site-selective oxygen isotopic substitution, performed on  $\text{YBa}_2\text{Cu}_3^{18}\text{O}_{6.2}$  samples. They found that in the starting  $^{18}\text{O}$  substituted sample, there is an isotopically shifted counterpart of the 595  $\text{cm}^{-1}$  mode at 567  $\text{cm}^{-1}$ , which disappears upon introducing  $^{16}\text{O}$  into the basal ( $\text{CuO}_x$ ) planes, and accompanied by the increase in intensity of the 595  $\text{cm}^{-1}$  line. This observation, together with symmetry arguments, led them to the conclusion that the two bands at 240 and 590  $\text{cm}^{-1}$ , are due to the *b*-axis vibrations of Cu(1) and O(1) atoms near the broken chain ends in full agreement with results of Thomsen *et al.* Pronounced correlations between these two bands, and superconducting properties of the films on which they appear, together with the conclusions of the works cited above allow us to state that they can be taken as Raman markers for imperfect chains within the grains of thin films.

It is worthy of mention that there is a large body of experimental and theoretical work, which establishes that the charge transfer between the  $\text{CuO}_x$  and  $\text{CuO}_2$  planes (and hence superconducting properties of the material) is determined mainly by the presence of sufficiently long  $\text{CuO}$  chains.<sup>38–43</sup> Furthermore, earlier infrared experiments performed on various underdoped and oxygen-doped YBCO ceramics with  $0.13 < \delta < 0.9$  have shown the existence of a strong mode at 585  $\text{cm}^{-1}$  the absorption of which is maximum for  $\delta < 0.4$  and diminishes drastically for  $\delta > 0.4$ .<sup>44,45</sup> This mode, therefore, should characterize the presence of oxygen defects in the  $\text{CuO}$  chains with infrared-allowed transitions.

However, we may argue that the exact nature of the 270–290  $\text{cm}^{-1}$  and 550–570  $\text{cm}^{-1}$  bands still remains somewhat unresolved in the Raman spectroscopy of YBCO-type materials. Even on samples with excellent electrophysical parameters, which prove the small concentration of point defects in the crystals, one may observe that a broad shoulder forms on the high-frequency side of the 500  $\text{cm}^{-1}$   $A_g$  mode. As a rule its intensity is not relatively high, but it increases dramatically upon high-temperature treatment of the sample, and can even mask the apex-oxygen mode in the spectra taken from

the *ab* plane.<sup>29,35,36,46</sup> Its spectral maximum is usually observed, as in our experiments, between 540 and 570  $\text{cm}^{-1}$ .

It is interesting to note that some of the reported frequencies of the  $B_{2g}$  and  $B_{3g}$  modes in orthorhombic YBCO samples match the two observed features, 270  $\text{cm}^{-1}$  for the  $B_{2g}$  mode of the O(4) atoms, and 560  $\text{cm}^{-1}$  for the  $B_{3g}$  mode of the plane O(2)/O(3) atoms. At first glance it is plausible to assume that we indeed have detected those same modes. We, however, rule this possibility out, since reported intensities of the  $B_{2g}$  and  $B_{3g}$  modes are about 2 orders of magnitude lower than those of the  $A_g$  modes.<sup>47</sup>

### E. Activation of forbidden phonon modes

Suppose that due to some kind of point defect or local atomic distortion the local point symmetry at atomic sites which are in the neighborhood of atomic defects is reduced in such a way that  $B_{2g}$  or  $B_{3g}$  modes can mix with the  $A_g$  vibrations of the perfect lattice. Then, assuming a small coupling, one may expect a mode of frequency near that of the corresponding  $B_{2g}$ - $B_{3g}$  mode (eventually slightly renormalized), but rather more intense, due to the mixing with the  $A_g$  atomic displacements, which by themselves modulate the dielectric susceptibility of the crystal. Extending this argument, we may speculate about the nature of such defects using group-subgroup correlation relations for the irreducible representations.<sup>48</sup> It is easy to establish that a necessary and sufficient condition to allow such mixing, is the loss of the  $\sigma_h$  mirror plane and at least one of the vertical mirror planes.

A simple physical model for such a situation is given in Fig. 10. Suppose that an apex atom jumps, due to the thermal excitation, from its normal O(4) position to the vacant O(5) position in the nearest basal plane. Before jumping the  $B_{3g}$  and the  $A_g$  modes have different transformation properties with respect to the  $\sigma_h$  and  $\sigma_v(x)$  planes, and thus no mixing between them is possible. After moving the atom to the new position, however, the only retained symmetry element is  $\sigma_v(y)$ , and the two displacement patterns have the same transformation properties, which, in principle allows their coupling. A similar situation may also occur when O(4) vacancy is in the neighborhood of the broken chain end, this time being activated in the  $B_{2g}$  counterpart. We also may expect that if this mechanism does take place, the  $A_g$  vibrations will couple the whole set of vibrations belonging to the same dispersion branch, as  $B_{2g}$  or  $B_{3g}$  ones, and instead of the  $\Gamma$ -point frequency one should observe a band which reflects the one-phonon density of states for the corresponding branch. This may account for the relatively large width of the 560  $\text{cm}^{-1}$  band. As indirect support for this mechanism, we can emphasize that during thin film growth, the temperature of the substrate is kept in the range 600–700 °C which is high enough to initiate atomic jumps from the O(4) and even O(2)/O(3) positions to the nearest interstitials.<sup>49</sup>

## VI. CONCLUSION

To summarize we have presented experimental and theoretical Raman spectra obtained from various

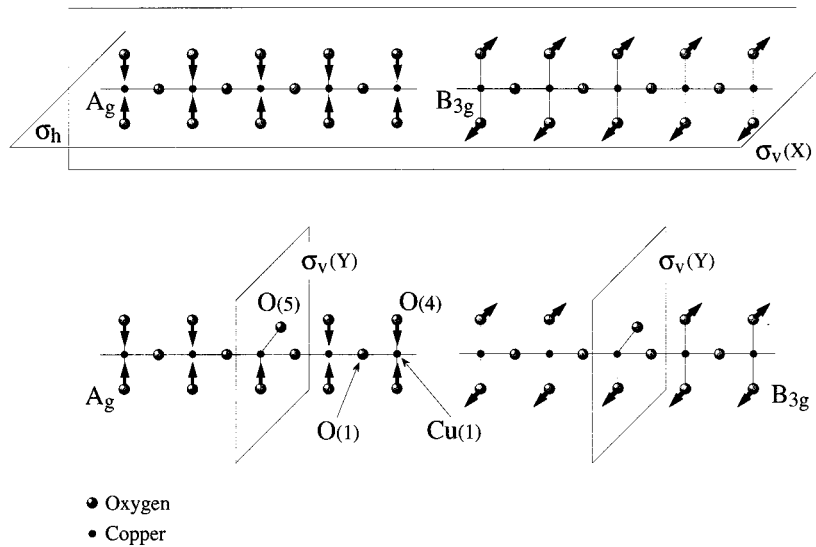


FIG. 10. The displacement pattern for the  $A_g$  and  $B_{3g}$  modes of the apex [O(4)] oxygen atoms. Notations are as usual: O(1) and Cu(1) for the chain oxygen and copper atoms, respectively, and O(5) for the otherwise vacant oxygen positions in the basal planes. It is clearly seen that upon jumping of an apex atom to an O(5) position the symmetry properties of the two modes become the same.

$Y(\text{Pr})\text{Ba}_2\text{Cu}_3\text{O}_{6+\delta}$  thin sputtered films ( $\delta \geq 0.5$ ). A temperature dependence study using the 1.83 eV excitation light has shown that anomalies of the oxygen phonons occur below  $T_c$  for  $\delta \approx 0.9$ . These anomalies indicate an intrinsic phenomenon linked to high- $T_c$  superconductivity and not to oxygen depletion or secondary phases. The detailed study of the fine structure of Ba and Cu bands in the Raman spectra has been performed with the help of a coupling model using a Green's function operator. Experimental results may be satisfactorily explained in the assumption of interaction between Ba and Cu(2) vibrations with a common continuum of low-energy interband excitations. Two hypotheses have been proposed for the origin of the continuum: transitions from the O(4)  $p_x$  to the O(4)  $p_y$  band near the  $RS$  line, and transitions from the chain to the odd plane band. The latter scenario implies the existence of an anisotropic superconducting gap. Additional incoherent contributions to the Raman spectra support the idea of a structural and electronic phase separation in optimally doped  $Y\text{Ba}_2\text{Cu}_3\text{O}_{6+\delta}$  materials. The changes of the baryum line vs temperature might be attributed to different environments due to oxygen depletion in the chains. We have shown that Raman spectra from these films, which are the signature of average macroscopic scattering

effects, may yield information about this microscopic oxygen depletion. In particular we have found that additional lines and forbidden phonon modes at 190, 220, 240, 290, 560, 590, and 600  $\text{cm}^{-1}$  disappear gradually in the Raman spectrum when the plasma in the sputtering process becomes richer in oxygen ions. These lines are thus good indicators of the oxygen defects in the chains. Finally, we conclude that microphase domains of  $\text{O}_{6.5}$  composition (ortho-II phase) may coexist in variable proportions with  $\text{O}_7$  ortho-I phase in these films and should be mainly responsible for their different electrophysical properties.

#### ACKNOWLEDGMENTS

The authors thank G. Garz and C. Gonzalez for having provided the films used in this study, and P. Bancel and S. de Vos for a reading of the manuscript. The Institut des Matériaux de Nantes is "Unité Mixte de Recherche No. 110 CNRS-Université de Nantes." This work was partially supported by Contract Nos. N F 2172 and F 2241 of the Bulgarian National Scientific Fund. The authors are indebted to Professor Iliev, Professor Lefrant, and Professor Rouxel for encouraging this work.

\*Permanent address: Faculty of Physics, Sofia University, 5 James Bourchier Blvd., BG 1126 Sofia, Bulgaria.

<sup>1</sup>E. Faulques, P. Mahot, M. Spiesser, T.P. Nguyen, G. Garz, C. Gonzalez, and P. Molinié, *Phys. Rev. B* **50**, 1209 (1994).

<sup>2</sup>C. Thomsen, in *Light Scattering in High  $T_c$  Superconductors*, Vol. 68 of *Topics in Applied Physics*, edited by M. Cardona and G. Guentherodt (Springer-Verlag, Berlin, 1991), and references therein; C. Thomsen, *Adv. Mater. B* **4**, 341 (1992); C. Thomsen and M. Cardona, in *Physical Properties of High-Temperature Superconductors*, edited by D.M. Ginsberg (World Scientific, Singapore, 1990).

<sup>3</sup>M. Cardona, *Physica C* **185**, 65 (1991).

<sup>4</sup>M. Balkanski, K.P. Jain, R. Besserman, and M. Jouanne, *Phys. Rev. B* **12**, 4328 (1975).

<sup>5</sup>M.V. Klein, in *Electronic Raman Scattering*, Vol. 68 of *Topics in Applied Physics*, edited by M. Cardona (Springer-Verlag, Berlin, 1975).

<sup>6</sup>X.K. Chen, E. Altendorf, J.C. Irwin, R. Liang, and W.N. Hardy, *Phys. Rev. B* **48**, 10 530 (1993).

<sup>7</sup>C. Thomsen, M. Cardona, B. Gegenheimer, R. Liu, and A. Simon, *Phys. Rev. B* **37**, 9860 (1988).

<sup>8</sup>S.L. Cooper, M.V. Klein, B.G. Pazol, J.P. Rice, and D.M. Ginsberg, *Phys. Rev. B* **37**, 5920 (1988).

<sup>9</sup>M. Cardona and C. Thomsen, in *High- $T_c$  Superconductors: Electronic Structure*, edited by A. Bianconi and A. Marcelli (Pergamon, Oxford, 1989), p. 79.

<sup>10</sup>C. Thomsen, R. Liu, M. Cardona, U. Amador, and E. Morain, *Solid State Commun.* **67**, 271 (1988).

<sup>11</sup>S.L. Cooper, F. Slakey, M.V. Klein, J.P. Rice, E.D. Bukowski, and D.M. Ginsberg, *Phys. Rev. B* **38**, 11 934 (1988).

<sup>12</sup>B. Friedl, C. Thomsen, and M. Cardona, *Phys. Rev. Lett.* **65**, 915 (1990).

<sup>13</sup>G. Bogachev, M.V. Abrashev, M.N. Iliev, N. Poulakis, E. Liar-

- okapis, C. Mitros, A. Koufoudakis, and V. Psyharis, *Phys. Rev. B* **49**, 12 151 (1994).
- <sup>14</sup>A. Mascarenhas, H. Katayama-Yoshida, J. Pankove, and S.K. Deb, *Phys. Rev. B* **39**, 4699 (1989).
- <sup>15</sup>T. Strach, T. Ruf, E. Schonherr, and M. Cardona, *Phys. Rev. B* **51**, 16 460 (1995).
- <sup>16</sup>E.T. Heyen, S.N. Rashkeev, I.I. Mazin, O.K. Andersen, R. Liu, M. Cardona, and O. Jepsen, *Phys. Rev. Lett.* **65**, 3048 (1990).
- <sup>17</sup>C.O. Rodriguez, A.I. Lichtenstein, I.I. Mazin, O. Jepsen, O. K. Andersen, and M. Methfessel, *Phys. Rev. B* **42**, 2692 (1990).
- <sup>18</sup>R.E. Cohen, W.E. Pickett, and H. Krakauer, *Phys. Rev. Lett.* **64**, 2575 (1990).
- <sup>19</sup>G. Garz, Ph.D. thesis, University of Paris XI, 1994. Also see the following papers concerning the fabrication of thin films: (a) G. Garz, T. Schild, N. Bouadma, F.R. Ladan, P. Gabelotaud, and C. Gonzalez, *Physica C* **235-240**, 3061 (1994); (b) C. Gonzalez, E. Faulques, G. Garz, P. Gabelotaud, and J.P. Senateur, *ibid.* **235-240**, 667 (1994), and references therein.
- <sup>20</sup>A. Bock, *Phys. Rev. B* **51**, 15 506 (1995).
- <sup>21</sup>U. Fano, *Phys. Rev.* **124**, 1866 (1961); F. Cerdeira, T.A. Fjedly, and M. Cardona, *Phys. Rev. B* **8**, 4734 (1973).
- <sup>22</sup>M.N. Iliev, C. Thomsen, V. Hadjiev, and M. Cardona, *Phys. Rev. B* **47**, 12 341 (1993).
- <sup>23</sup>V.G. Hadjiev, C. Thomsen, J. Kircher, and M. Cardona, *Phys. Rev. B* **47**, 9148 (1993).
- <sup>24</sup>V.G. Ivanov and M.N. Iliev, *Physica C* **244**, 293 (1995).
- <sup>25</sup>I.I. Mazin, S.N. Rashkeev, A.L. Liechtenstein, and O. K. Andersen, *Phys. Rev. B* **46**, 11 232 (1992).
- <sup>26</sup>H. Monien and A. Zawadowski, *Phys. Rev. Lett.* **63**, 911 (1989).
- <sup>27</sup>N. Pyka, W. Reichardt, L. Pinschovius, G. Engel, J. Rossat-Mignod, and J.Y. Henry, *Phys. Rev. Lett.* **70**, 1457 (1993).
- <sup>28</sup>R. Feile, *Physica C* **159**, 1 (1989).
- <sup>29</sup>G. Burns, F.H. Dacol, C. Feild, and F. Holtzberg, *Solid State Commun.* **77**, 367 (1991); **75**, 893 (1990).
- <sup>30</sup>M.V. Belousov, I.V. Ignat'ev, N.V. Orekhova, and V.Yu. Davydov, *Sov. Phys. Solid State* **34**, 1500 (1992).
- <sup>31</sup>A. Sacuto, Ph.D. thesis, University of Paris VI, 1992; A. Sacuto, M.A. Kanehisa, and O. Gorokov, *J. Phys. Condens. Matter* **6**, 1057 (1994).
- <sup>32</sup>Fred Pollack, in *Analytical Raman Spectroscopy*, edited by Jeanette G. Grasselli and B.J. Bulkin, Chemical Analysis Series Vol. 114 (Wiley, New York, 1991).
- <sup>33</sup>C. Thomsen, M. Cardona, B. Gegenheimer, R. Liu, and A. Simon, *Phys. Rev. B* **37**, 9860 (1988).
- <sup>34</sup>D.R. Wake, F. Slakey, M.V. Klein, J.P. Rice, and D.M. Ginsberg, *Phys. Rev. Lett.* **67**, 3728 (1991).
- <sup>35</sup>K.F. McCarty, J.C. Hamilton, R.N. Shelton, and D.S. Ginley, *Phys. Rev. B* **38**, 2914 (1988).
- <sup>36</sup>S. Fantini, L. Ulivi, and M. Zoppi, *Solid State Commun.* **93**, 519 (1995).
- <sup>37</sup>V.G. Ivanov, M.N. Iliev, and C. Thomsen, *Phys. Rev. B* **52**, 13 652 (1995).
- <sup>38</sup>B.W. Veal and A.P. Paulicas, *Physica C* **184**, 321 (1991).
- <sup>39</sup>J.D. Jorgensen, Shyuou Pei, P. Lightfoot, Hao Shi, A.P. Paulicas, and B.W. Veal, *Physica C* **167**, 571 (1990).
- <sup>40</sup>C. Picard and P. Gerdanian, *Physica C* **196**, 297 (1992).
- <sup>41</sup>I.N. Kuropyatnik and A.N. Lavrov, *Physica C* **197**, 47 (1992).
- <sup>42</sup>J.K. Burgett, *Physica C* **191**, 282 (1992).
- <sup>43</sup>H.F. Pulsen, N.H. Andersen, J.V. Andersen, H. Bohr, and O.G. Mouritsen, *Nature* **349**, 595 (1991).
- <sup>44</sup>H. Kuzmany, M. Matus, E. Faulques, S. Pekker, Gy. Hutiray, S. Zsoldos, and L. Mihaly, *Solid State Commun.* **65**, 1343 (1988).
- <sup>45</sup>H. Kuzmany, M. Matus, E. Faulques, S. Pekker, Gy. Hutiray, S. Zsoldos, and L. Mihaly, *Phys. Scr.* **T25**, 82 (1989).
- <sup>46</sup>V.G. Ivanov, V.G. Hadjiev, and M.N. Iliev, *Physica C* **235-240**, 1255 (1994).
- <sup>47</sup>K.F. McCarty, J.Z. Liu, R.N. Shelton, and H.B. Radousky, *Phys. Rev. B* **41**, 8792 (1990).
- <sup>48</sup>H. Poulet and J.P. Mathieu, *Vibrational Spectra and Symmetry of Crystals* (Gordon and Breach, New York, 1970).
- <sup>49</sup>K. Conder, E. Kaldis, J. Maciejewski, K.A. Müller, and E.F. Steigmeier, *Physica C* **210**, 282 (1993).